

Azimuthal Angular Correlation of J/ψ Plus Jet Production at the EIC

Luca Maxia^{1,*} and Feng Yuan^{2,†}

¹*Van Swinderen Institute for Particle Physics and Gravity,
University of Groningen, Nijenborgh 4, 9747 AG Groningen, The Netherlands*

²*Nuclear Science Division, Lawrence Berkeley National Laboratory, Berkeley, CA 94720, USA*

By investigating the soft gluon radiation in the J/ψ plus jet photoproduction at the electron-ion collider (EIC), we demonstrate that the azimuthal angular correlations between the leading jet and heavy quarkonium provide a unique probe to the production mechanism of the latter. In particular, a significant $\cos(\phi)$ asymmetry is found for the color-singlet channel, whereas it vanishes or has an opposite sign for color-octet production, depending on the jet transverse momentum. Numerical results of $\cos(\phi)$ and $\cos(2\phi)$ asymmetries employing both the color-singlet model and the nonrelativistic QCD approach are presented for typical kinematics at the future EIC.

Introduction. In recent years, heavy quarkonium production in various inclusive processes has attracted great interest as a way to probe gluon distributions both in initial (nucleon tomography) and final (fragmentation functions) states [1–17]. Among them, Refs. [10, 12] have studied the azimuthal angular correlation in semi-inclusive DIS between J/ψ and leading jet to probe the so-called linearly polarized gluon distribution. In this paper, we will investigate the dominant contributions from the soft gluon radiations and demonstrate that azimuthal correlations can also provide a unique opportunity to disentangle between the color-singlet (CS) and color-octet (CO) mechanisms.

In the nonrelativistic QCD (NRQCD) [18] approach, the heavy-quark pair forms a Fock state specified by $n = 2S+1 L_J^{[c]}$, with S denoting its spin, L the orbital angular momentum, J the total angular momentum and c its color. Note that, within this framework, the pair can couple either as a CS or CO state. Therefore, comprehending the significance of the CS and CO contributions is crucial. Although great progress has been made in understanding heavy quarkonium production in hadronic collisions (for recent reviews see [19, 20]), challenges remain to phenomenologically describe quarkonium formation and, in particular, to distinguish between these two mechanisms.

In this regard, we will demonstrate how azimuthal angular correlations in J/ψ plus jet photoproduction at the electron-ion collider (EIC) offer a unique probe of the underlying production mechanism. In particular, we will show that these correlations significantly differ between the CS and CO channels. We will focus on the correlation kinematics, i.e., the transverse momentum of individual particles is much larger than the total transverse momentum. Therefore, by combining the transverse momenta of the J/ψ and the jet, $k_{\psi\perp}$ and $k_{j\perp}$ respectively, we can identify two scales. The first one is given by $\vec{P}_\perp = \frac{\vec{k}_{\psi\perp} - \vec{k}_{j\perp}}{2}$, while the second by $\vec{q}_\perp = \vec{k}_{\psi\perp} + \vec{k}_{j\perp}$, with $|\vec{q}_\perp| \ll |\vec{P}_\perp|$. Hence, according to this limit, the

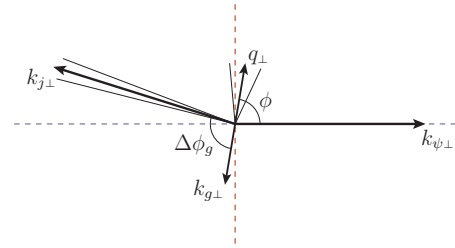


FIG. 1. Kinematic correlation between the leading jet and heavy quarkonium as viewed in the transverse plane. Here q_\perp (the total outgoing transverse momentum) is small compared to individual transverse momenta.

heavy quarkonium and jet are mainly produced back-to-back in the transverse plane (see Fig. 1). An imbalance between the two final-state particles with nonzero $|\vec{q}_\perp|$ can be generated by high-order perturbative corrections and from the intrinsic transverse momentum of the incoming parton. We identify this imbalance with the angle ϕ , namely the difference between the azimuthal angles of \vec{q}_\perp and $\vec{k}_{\psi\perp}$, where we can approximate the latter as $\vec{k}_{\psi\perp} \approx \vec{P}_\perp$ within the correlation limit.

Moreover, we remark that in this limit such azimuthal imbalance is mostly generated from the soft/collinear gluon radiation from perturbative diagrams (see for instance Ref. [21, 22]). This contribution, denoted by $k_{g\perp}$ in Fig. 1, tends to align with the jet direction at low q_\perp , which leads to significant $\cos(n\phi)$ asymmetries. Detailed examples have been shown for vector boson (photon/Z/Higgs) plus jet production in pp collisions [23, 24] and for lepton plus jet [21] and dijet [22] productions in ep collisions. Nonetheless, this feature is also particularly interesting to investigate the production mechanism of quarkonia.

With this paper, we suggest exploiting azimuthal angular distributions, especially the $\cos(\phi)$ and $\cos(2\phi)$, to unravel the production mechanism. Such findings can

* l.maxia@rug.nl

† fyuan@lbl.gov

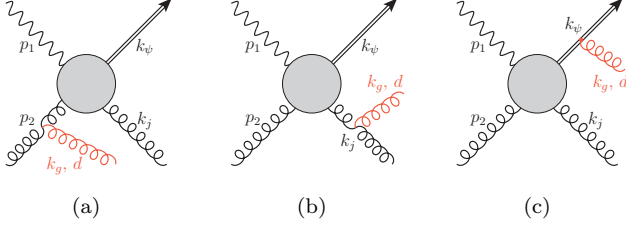


FIG. 2. *Soft gluon radiation in the J/ψ plus jet photoproduction process. All three diagrams contribute to the color-octet channel, whilst only the first two on the left are relevant for the color-singlet one.*

then be applied to electroproduction to investigate gluon distributions (e.g. linearly polarized gluons) in nucleons and nuclei.

Soft gluon radiation at one loop. In this section we discuss the implication of azimuthal correlation between the J/ψ and jet for photoproduction at the future EIC, $\gamma p \rightarrow J/\psi + jet + X$. The leading-order (LO) NRQCD contribution comes from the photon-gluon fusion partonic process, namely

$$\gamma(p_1) + g(p_2) \rightarrow [Q\bar{Q}]^{(1,8)}(k_\psi) + g(k_j), \quad (1)$$

where the momentum of each particle is given in the parenthesis. Moreover, the heavy-quark pair $Q\bar{Q}$ can be either in a CS (labeled with (1)) or CO (labeled with (8)) configuration. At this order, the J/ψ and jet are back-to-back in the transverse plane, so that $q_\perp = 0$. However, at higher orders, small nonzero q_\perp originates from parton intrinsic transverse momenta and soft gluon radiation. In the following, we will derive the LO soft gluon radiation contribution and the associated azimuthal angular asymmetries (Fig. 2), whereas the collinear gluon radiation can be factorized into the TMD gluon distributions.

The major difference between CS and CO channels is that the soft gluon radiation associated with the heavy quark pair only contributes to the latter. This occurs due to cancellations between the emissions from the heavy quark and antiquark when the pair is in a CS state. This difference has significant implications for the azimuthal asymmetries, as we will discuss in the following.

By adding Fig. 2a and Fig. 2b we obtain the amplitude squared (averaged over the color and spin of incoming particles) for the soft gluon radiation in the CS channel:

$$|\overline{\mathcal{A}}_1^{(1)}|^2 = g_s^2 C_A S_g(p_2, k_j) |\overline{\mathcal{A}}_0^{(1)}|^2, \quad (2)$$

where $A_0^{(1)}$ is the LO amplitude and $S_g(v_a, v_b)$ is a shorthand notation for

$$S_g(v_a, v_b) = \frac{2(v_a \cdot v_b)}{(v_a \cdot k_g)(v_b \cdot k_g)}. \quad (3)$$

Integration over the phase space of the emitted soft

gluon follows that in Ref. [21, 22, 25–28], leading to

$$\int \frac{d^3 k_g}{(2\pi)^3 2E_{k_g}} |\overline{\mathcal{A}}_1^{(1)}|^2 \delta^{(2)}(q_\perp + k_{g\perp}) = \frac{\alpha_s C_A}{2\pi^2 |\vec{q}_\perp|^2} |\overline{\mathcal{A}}_0^{(1)}|^2 \left[\ln \frac{\hat{s}}{|\vec{q}_\perp|^2} + \ln \frac{\hat{t}}{\hat{u}} + I_j(R, \phi) \right], \quad (4)$$

where $\hat{s} = (p_1 + p_2)^2$, $\hat{t} = (p_2 - k_j)^2$ and $\hat{u} = (p_1 - k_j)^2$. The first term in the bracket is the double logarithm (in b_T -space) that provides the dominant behavior at low q_\perp . The second logarithm, $\ln(\hat{t}/\hat{u})$, depends on the jet rapidity. The third term, I_j , is one of the subjects of this work, being the azimuthal distribution that arises from the soft gluon radiation. As a result of the removal of collinear divergences already included within the jet function, I_j depends on the jet size R . To further investigate this distribution, we expand it in a Fourier series according to

$$I_j(R, \phi) = C_0^{(j)}(R) + 2 \sum_{n=1}^{\infty} C_n^{(j)}(R) \cos(n\phi). \quad (5)$$

In line with previous works, we find that the soft gluon radiation associated with the jet leads to a dominant $\cos(\phi)$ asymmetry, with the $\cos(2\phi)$ one being much smaller.

At variance with the CS case, when the pair forms a CO state all diagrams in Fig. 2 are relevant. Independently from the color structures of the LO partonic process, one gluon radiation leads to the same contribution. While it is straightforward to prove that the first two diagrams do not depend on the Fock state, it is worthwhile to provide further elaboration on the last one (Fig. 2c), which corresponds to soft gluon radiation from the heavy-quark pair itself. Within NRQCD, the total soft gluon radiation from the quark and antiquark lines is given by $g_s \frac{k_\psi^\mu}{k_g \cdot k_\psi + i\epsilon} (\Phi_{ij} T^d - T^d \Phi_{ij}) \Gamma$ [13, 29], where Φ represents the wave function of the pair, i (j) and d are respectively the color indices for the quark (antiquark) and the radiated soft gluon, μ is connected to the soft gluon polarization vector, and Γ stands for other hard parts coming from the scattering amplitude. The minus sign in the second term comes from the interaction with the antiquark which is opposite to that with the quark. When the pair forms a CO state, the color matrix of the wave function can be parameterized as $\Phi_{ij}^{(8,c)} \propto T_{ij}^c$, where $c = 1, \dots, 8$ represents the color index of the pair. The sum of the two diagrams will then be proportional to $g_s \frac{k_\psi^\mu}{k_g \cdot k_\psi + i\epsilon} (-if'_{cd}) \Phi^{(8,c)} \Gamma^{c'}$, where we emphasized that the pair coupled with the rest of the diagram with a different color index c' before the soft gluon emission. Note that we have not taken any assumption on the spin and angular configuration entering in Φ , which implies that the result is independent of those quantum numbers. Moreover, the found result is similar to that for soft gluon radiation from a gluon jet in the final state [26]. The only difference originates from the gluon on-shell condition, $k^2 = 0$ for jets and $k^2 = M_V^2 \approx 4M_Q^2$ for quarkonia.

By including the soft gluon radiations from the initial and final state gluons (Figs. 2a and 2b), the averaged CO amplitude squared is summarized as follows

$$|\overline{\mathcal{A}}_1^{(8)}|^2 = g_s^2 C_A \left[S_g(p_2, k_j) + \frac{1}{2} \left(S_g(p_2, k_\psi) - S_g(k_\psi, k_\psi) + S_g(k_j, k_\psi) - S_g(p_2, k_j) \right) \right] |\overline{\mathcal{A}}_0^{g,(8)}|^2, \quad (6)$$

where $\overline{\mathcal{A}}_0^{g,(8)}$ represents the LO (gluon) amplitude. In principle, $|\overline{\mathcal{A}}_1^{(8)}|^2$ depends on quarks too. However, we will neglect the quark contribution in the following, since it is reasonable to expect that it will be suppressed compared to the gluon one. Note that the first term of Eq. (6) is equivalent to that in Eq. (2) for the CS case and, therefore, is a contribution purely driven by the gluon jet. Consequently, all the terms in the round brackets can be associated with the J/ψ .

From Eq. (6), the integration over the phase space of the emitted soft gluon gives

$$\begin{aligned} & \int \frac{d^3 k_g}{(2\pi)^3 2E_{k_g}} |\overline{\mathcal{A}}_1^{(8)}|^2 \delta^{(2)}(q_\perp + k_{g\perp}) \\ &= \frac{\alpha_s C_A}{2\pi^2 |\vec{q}_\perp|^2} |\overline{\mathcal{A}}_0^{g,(8)}|^2 \left[\ln \frac{\hat{s}}{|\vec{q}_\perp|^2} + \frac{1}{2} \ln \frac{1 - M_\psi^2/\hat{u}}{1 - M_\psi^2/\hat{t}} \right. \\ &+ I_j(R, \phi) + I_\psi(m_{\psi\perp}, \phi) + \frac{1}{2} I_{\psi-j}(m_{\psi\perp}, \Delta y, 2\phi) \\ &\left. - \frac{1}{2} I_\psi^{\text{jet}}(R, m_{\psi\perp}, \Delta y, \phi) \right], \quad (7) \end{aligned}$$

where we have introduced $m_{\psi\perp} = M_\psi/k_{\psi\perp}$, while $\Delta y = y_\psi - y_j$ is the rapidity difference between the J/ψ (y_ψ) and the leading jet (y_j). The first term of Eq. (7) corresponds to the leading, double logarithmic behavior at low q_\perp , which is the same as the CS case. This implies that the soft gluon emission from the (massive) quarkonium does not provide double logarithms, a conclusion in line with other works [13, 30–34]. The second term comes from the sum of rapidities $y_j + y_\psi$, which differs from zero due to the presence of the J/ψ mass. The third term, I_j , is the same azimuthal dependence associated with the jet in Eq. (4), and its Fourier expansion follows Eq. (5). The last three azimuthal distributions, I_ψ , $I_{\psi-j}$ and I_ψ^{jet} , are the novel terms due to the production of a CO state. Their definitions and derivations are in the supplemental material. Again, we expand them in terms of $\cos(n\phi)$ harmonics according to

$$I_{[\psi]}(K, \phi) = C_0^{([\psi])}(K) + 2 \sum_{n=1}^{\infty} C_n^{([\psi])}(K) \cos(n\phi), \quad (8)$$

where $I_{[\psi]}$ is either I_ψ , $I_{\psi-j}$ or I_ψ^{jet} , and K is a short-hand notation for the dependence on the kinematical variables of each distribution.

Mechanism	$C_0^{(c)}$	$C_1^{(c)}$	$C_2^{(c)}$
CS	0.89	2.61	0.95
CO ($m_{\psi\perp} = 0.26$)	2.46	-0.02	1.72
CO ($m_{\psi\perp} = 0.1$)	3.40	-1.80	3.28

TABLE I. First coefficients of the azimuthal correlation Fourier expansions for the CS and CO mechanisms with $R = 0.4$. Note that the coefficients within the CS channel are independent of $k_{j\perp}$.

Summarizing the above results, the differential cross section including the soft gluon radiation in the correlation limit is given by

$$\begin{aligned} \frac{d^4 \sigma^{(1,8)}}{d\Omega} &= \sigma_0^{(1,8)} x_g f_g(x_g) \frac{\alpha_s C_A}{2\pi^2 |\vec{q}_\perp|^2} \left[\ln \frac{\hat{s}}{|\vec{q}_\perp|^2} \right. \\ &\left. + 2 \sum_{n=0}^{\infty} C_n^{(1,8)}(R, m_{\psi\perp}, \Delta y = 0) \cos(n\phi) \right], \quad (9) \end{aligned}$$

where $\sigma_0^{(1,8)}$ represents the LO cross section [35], $d\Omega \equiv dy_j dy_\psi d^2 \vec{P}_\perp d^2 \vec{q}_\perp$ the phase space, and $f_g(x_g)$ is the gluon distribution. Moreover, we are considering the case where $y_j = y_\psi = 0$ for simplicity, since this scenario does not present additional, non-divergent logarithms. Hence, in Eq. (9) we have that the first term corresponds to the leading double logarithm, while the second line stands for the single logarithms. Since the latter carries the azimuthal dependence, we have already expanded it into harmonics, with the coefficients $C_n^{(1,8)}$ connected to those in the Fourier series of each distribution. Therefore they depend on the jet size R , the heavy quarkonium mass via $m_{\psi\perp} = M_\psi/P_\perp$ and the rapidity difference $\Delta y = y_\psi - y_j$. Most importantly, these coefficients depend crucially on the production channel considered. To illustrate these differences, we consider typical kinematics for future EIC measurements. We take $R = 0.4$ and $m_{\psi\perp} = 0.26, 0.1$, that correspond to $k_{j\perp} \approx 12, 30$ GeV. Within these choices, the first three coefficients of the Fourier expansion in Eq. (9) are given in Table I, displaying a clear difference between CS and CO channels. In particular, the coefficient $C_1^{(1)}$ is significantly positive due to the soft gluon radiation associated with the jet in the final state. However, the soft gluon radiation associated with heavy quark pair has an opposite sign. Thus, a proper choice of $m_{\psi\perp}$ can reduce the magnitude, or even change the sign, of $C_1^{(8)}$ when compared to $C_1^{(1)}$, while on the other hand $C_2^{(8)}$ and $C_2^{(1)}$ stay of more or less the same order. For more details on the comparison between the CS and CO channels we refer the reader to the supplemental materials.

All order resummation and predictions for the EIC. All order resummation is needed to make reliable

predictions for the soft gluon radiation contributions. Following the standard TMD framework, we have

$$\frac{d^4\sigma^{(1,8)}}{d\Omega} = \sigma_0^{(1,8)} \int \frac{|\vec{b}_\perp| d|\vec{b}_\perp|}{(2\pi)} \left[J_0(|\vec{b}_\perp||\vec{q}_\perp|) \widetilde{W}_0^{(1,8)}(|\vec{b}_\perp|) + 2 J_n(|\vec{b}_\perp||\vec{q}_\perp|) \widetilde{W}_n^{(1,8)}(|\vec{b}_\perp|) \cos(n\phi) \right], \quad (10)$$

where

$$\widetilde{W}_0^{(1,8)}(|\vec{b}_\perp|) = x_g f_g(x_g, \mu_b) e^{-S^{(1,8)}(P_\perp, b_\perp)}, \quad (11)$$

and

$$\widetilde{W}_n^{(1,8)}(|\vec{b}_\perp|) = \frac{C_A \alpha_s}{n\pi} C_n^{(1,8)} \widetilde{W}_0^{(1,8)}(|\vec{b}_\perp|). \quad (12)$$

Note that in Eq. (10) we have already included higher-order double logarithmic corrections present also for the angular dependent term [23, 24]. The Sudakov form factor $S(P_\perp, b_\perp)$ is separated into perturbative and non-perturbative parts: $S(P_\perp, b_\perp) = S_{\text{pert.}}(P_\perp, b_\perp) + S_{\text{NP}}(P_\perp, b_\perp)$. The perturbative part at one loop is defined as

$$S_{\text{pert.}}^{(1,8)} = \int_{\mu_0^2}^{\hat{s}} \frac{d\mu^2}{\mu^2} \frac{\alpha_s C_A}{2\pi} \left[\ln \frac{\hat{s}}{\mu^2} - 2\beta_0 + 2C_0^{(1,8)} \right], \quad (13)$$

where $\beta_0 = 11/12 - N_f/18$ and $\mu_b = b_0/b_\perp$ with $b_0 = 2e^{\Gamma_E}$ and Γ_E being the Euler's constant. Moreover, in Eq. (13) we have already introduced the b_* -prescription [36], where $b_* = b_\perp / \sqrt{1 + (b_\perp/b_{\text{max}})^2}$ with $b_{\text{max}} = 1.5$ GeV. For the non-perturbative part, we have contributions driven by the incoming gluon and the outgoing jet and quarkonium. For the first one, we employ the non-perturbative Sudakov found for TMD quark distributions in Refs. [37, 38] with the appropriate Casimir scaling

$$S_{\text{NP}}^g = \frac{C_A}{C_F} \left[0.106 b_\perp^2 + 0.42 \ln \frac{P_\perp}{Q_0} \ln \frac{b_\perp}{b_*} \right], \quad (14)$$

where $Q_0^2 = 2.4$ GeV². For the others, we assume that the non-perturbative contribution associated with the jet is given by $S_{\text{NP}}^{\text{jet}} = g_\Lambda^{\text{jet}} b_\perp^2$, and the J/ψ one by $S_{\text{NP}}^\psi = g_\Lambda^\psi b_\perp^2$. Overall, we employ $S_{\text{NP}}^{(1)} = S_{\text{NP}}^g + S_{\text{NP}}^{\text{jet}}$ for the CS mechanism and $S_{\text{NP}}^{(8)} = S_{\text{NP}}^g + S_{\text{NP}}^{\text{jet}} + S_{\text{NP}}^\psi$ for the CO channel, with $g_\Lambda^{\text{jet}} = g_\Lambda^\psi = 0.225$ GeV², a choice in line with [21, 22]. We also checked that the final azimuthal asymmetries do not depend significantly on these parameters, as expected.

From the above expressions, we find that the azimuthal asymmetries of $\cos(\phi)$ and $\cos(2\phi)$ are linearly proportional to the respective $C_{1,2}$ coefficients which are different between the CS and CO channels. Therefore, they can be used to probe these two production mechanisms.

As an example, in Fig. 3, we show the numerical results for $\langle \cos(\phi) \rangle$ and $\langle \cos(2\phi) \rangle$ as functions of q_\perp for kinematics accessible at the EIC, with $\sqrt{s_{\gamma p}} = 100$ GeV, $R = 0.4$

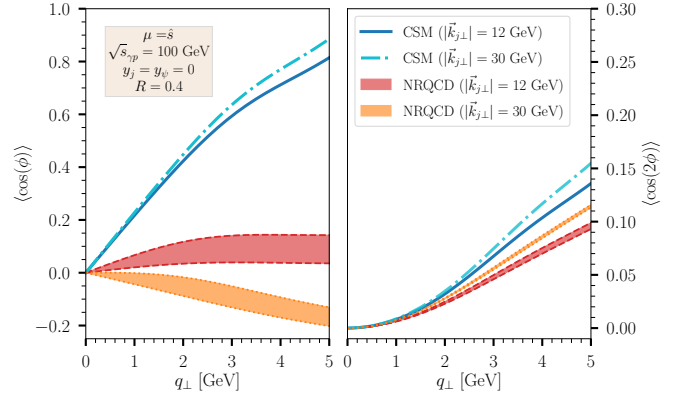


FIG. 3. Averaged resummed azimuthal asymmetries for J/ψ plus jet photoproduction at $\sqrt{s_{\gamma p}} = 100$ GeV. Solid blue and dash-dotted cyan lines are the CSM predictions at $|\vec{k}_{j\perp}| = 12$ GeV and $|\vec{k}_{j\perp}| = 30$ GeV, whereas for the NRQCD approach we have the dashed red and dotted orange lines, respectively. Bands are obtained by combining the results from different LDMEs central values. Jet size is $R = 0.4$ in all cases.

and $|\vec{k}_{j\perp}| = 12, 30$ GeV. For the parton distribution function we have employed the MSHT20 LO set [39]. Predictions are shown for both the color-singlet model (CSM) and NRQCD approach, with the latter mainly depending on the relative fraction of the CS and total CO contributions. Indeed, note that NRQCD predictions are not strongly dependent on the individual CO long-distance matrix elements (LDMEs), as can be understood from the bands in Fig. 3 which are constructed by combining several central values of the associated LDMEs from different global analyses [40–44].

As expected, the resummed form of $\langle \cos(n\phi) \rangle$ is exactly 0 at $q_\perp = 0$, and at small q_\perp they scale as $\langle \cos(n\phi) \rangle \propto q_\perp^n$ [24]. At large q_\perp , we expect they will decrease as functions of q_\perp , where the hard gluon radiation dominates and there is no preferred direction. This will modify the behavior of both $\langle \cos(\phi) \rangle$ and $\langle \cos(2\phi) \rangle$ asymmetries at large q_\perp in Fig. 3. Meanwhile, this figure shows a distinct behavior between $\langle \cos(\phi) \rangle$ and $\langle \cos(2\phi) \rangle$ predictions. Indeed, the former highly depends on the model considered, whereas the CSM and NRQCD outcomes are comparable, and in general non-negligible, for $\langle \cos(2\phi) \rangle$. As demonstrated, such differences offer a unique opportunity to determine the underlying quarkonium production mechanism.

Conclusions. In summary, we have demonstrated that the soft gluon radiation leads to significantly different azimuthal angular correlations between the CS and CO mechanisms in the J/ψ plus jet photoproduction process at the future EIC. This directly affects azimuthal asymmetry predictions within the CSM and the NRQCD approach, where the latter presents a soft dependence on the LDME. Thus, we consider these observables as the stems to disentangle these two production mechanisms. We also expect that similar conclusions can be drawn for

other experiments as well, like in hadronic processes at the LHC. Moreover, $\cos(2\phi)$ has been proposed to study the linearly polarized gluon distribution in the electroproduction of J/ψ plus jet at the EIC. We expect that the soft gluon radiation will lead to sizable contributions to $\cos(2\phi)$ asymmetry in this process as well, with a behavior similar to that shown in Fig. 3 for photoproduction. Understanding the soft gluon radiation will be a crucial step to unambiguously determine the gluon tomography of linearly polarized distribution from this measurement.

We will explore all these physics, including higher-order perturbative and power corrections, in the future.

ACKNOWLEDGMENTS

We thank Prof. D. Boer for the valuable discussions. This material is based upon work supported by the U.S. Department of Energy, Office of Science, Office of Nuclear Physics, under contract numbers DE-AC02-05CH11231.

-
- [1] R. M. Godbole, A. Misra, A. Mukherjee, and V. S. Rawaot, *Phys. Rev. D* **85**, 094013 (2012), arXiv:1201.1066 [hep-ph].
- [2] D. Boer and C. Pisano, *Phys. Rev. D* **86**, 094007 (2012), arXiv:1208.3642 [hep-ph].
- [3] R. M. Godbole, A. Misra, A. Mukherjee, and V. S. Rawaot, *Phys. Rev. D* **88**, 014029 (2013), arXiv:1304.2584 [hep-ph].
- [4] W. J. den Dunnen, J. P. Lansberg, C. Pisano, and M. Schlegel, *Phys. Rev. Lett.* **112**, 212001 (2014), arXiv:1401.7611 [hep-ph].
- [5] A. Mukherjee and S. Rajesh, *Phys. Rev. D* **93**, 054018 (2016), arXiv:1511.04319 [hep-ph].
- [6] A. Mukherjee and S. Rajesh, *Phys. Rev. D* **95**, 034039 (2017), arXiv:1611.05974 [hep-ph].
- [7] A. Mukherjee and S. Rajesh, *Eur. Phys. J. C* **77**, 854 (2017), arXiv:1609.05596 [hep-ph].
- [8] S. Rajesh, R. Kishore, and A. Mukherjee, *Phys. Rev. D* **98**, 014007 (2018), arXiv:1802.10359 [hep-ph].
- [9] F. Scarpa, D. Boer, M. G. Echevarria, J.-P. Lansberg, C. Pisano, and M. Schlegel, *Eur. Phys. J. C* **80**, 87 (2020), arXiv:1909.05769 [hep-ph].
- [10] U. D'Alesio, F. Murgia, C. Pisano, and P. Tael, *Phys. Rev. D* **100**, 094016 (2019), arXiv:1908.00446 [hep-ph].
- [11] R. Kishore, A. Mukherjee, and M. Siddiqah, *Phys. Rev. D* **104**, 094015 (2021), arXiv:2103.09070 [hep-ph].
- [12] R. Kishore, A. Mukherjee, A. Pawar, and M. Siddiqah, *Phys. Rev. D* **106**, 034009 (2022), arXiv:2203.13516 [hep-ph].
- [13] D. Boer, J. Bor, L. Maxia, C. Pisano, and F. Yuan, *JHEP* **08**, 105 (2023), arXiv:2304.09473 [hep-ph].
- [14] M. Copeland, S. Fleming, R. Gupta, R. Hodges, and T. Mehen, (2023), arXiv:2308.08605 [hep-ph].
- [15] M. G. Echevarria, S. F. Romera, and I. Scimemi, (2023), arXiv:2308.12356 [hep-ph].
- [16] M. Copeland, S. Fleming, R. Gupta, R. Hodges, and T. Mehen, (2023), arXiv:2310.13737 [hep-ph].
- [17] Z.-B. Kang, E. Li, and F. Salazar, (2023), arXiv:2310.12102 [hep-ph].
- [18] G. T. Bodwin, E. Braaten, and G. P. Lepage, *Phys. Rev. D* **51**, 1125 (1995), [Erratum: *Phys.Rev.D* 55, 5853 (1997)], arXiv:hep-ph/9407339.
- [19] N. Brambilla *et al.*, *Eur. Phys. J. C* **71**, 1534 (2011), arXiv:1010.5827 [hep-ph].
- [20] J.-P. Lansberg, *Phys. Rept.* **889**, 1 (2020), arXiv:1903.09185 [hep-ph].
- [21] Y. Hatta, B.-W. Xiao, F. Yuan, and J. Zhou, *Phys. Rev. Lett.* **126**, 142001 (2021), arXiv:2010.10774 [hep-ph].
- [22] Y. Hatta, B.-W. Xiao, F. Yuan, and J. Zhou, *Phys. Rev. D* **104**, 054037 (2021), arXiv:2106.05307 [hep-ph].
- [23] S. Catani, M. Grazzini, and A. Torre, *Nucl. Phys. B* **890**, 518 (2014), arXiv:1408.4564 [hep-ph].
- [24] S. Catani, M. Grazzini, and H. Sargsyan, *JHEP* **06**, 017 (2017), arXiv:1703.08468 [hep-ph].
- [25] P. Sun, C. P. Yuan, and F. Yuan, *Phys. Rev. Lett.* **113**, 232001 (2014), arXiv:1405.1105 [hep-ph].
- [26] P. Sun, C. P. Yuan, and F. Yuan, *Phys. Rev. D* **92**, 094007 (2015), arXiv:1506.06170 [hep-ph].
- [27] X. Liu, F. Ringer, W. Vogelsang, and F. Yuan, *Phys. Rev. Lett.* **122**, 192003 (2019), arXiv:1812.08077 [hep-ph].
- [28] X. Liu, F. Ringer, W. Vogelsang, and F. Yuan, *Phys. Rev. D* **102**, 094022 (2020), arXiv:2007.12866 [hep-ph].
- [29] F. Yuan, *Phys. Rev. D* **78**, 014024 (2008), arXiv:0801.4357 [hep-ph].
- [30] P. Sun, C. P. Yuan, and F. Yuan, *Phys. Rev. D* **88**, 054008 (2013), arXiv:1210.3432 [hep-ph].
- [31] H. X. Zhu, C. S. Li, H. T. Li, D. Y. Shao, and L. L. Yang, *Phys. Rev. Lett.* **110**, 082001 (2013), arXiv:1208.5774 [hep-ph].
- [32] R. Zhu, P. Sun, and F. Yuan, *Phys. Lett. B* **727**, 474 (2013), arXiv:1309.0780 [hep-ph].
- [33] M. G. Echevarria, *JHEP* **10**, 144 (2019), arXiv:1907.06494 [hep-ph].
- [34] S. Fleming, Y. Makris, and T. Mehen, *JHEP* **04**, 122 (2020), arXiv:1910.03586 [hep-ph].
- [35] P. Ko, J. Lee, and H. S. Song, *Phys. Rev. D* **54**, 4312 (1996), [Erratum: *Phys.Rev.D* 60, 119902 (1999)], arXiv:hep-ph/9602223.
- [36] J. C. Collins, D. E. Soper, and G. F. Sterman, *Nucl. Phys. B* **250**, 199 (1985).
- [37] P. Sun, J. Isaacson, C. P. Yuan, and F. Yuan, *Int. J. Mod. Phys. A* **33**, 1841006 (2018), arXiv:1406.3073 [hep-ph].
- [38] A. Prokudin, P. Sun, and F. Yuan, *Phys. Lett. B* **750**, 533 (2015), arXiv:1505.05588 [hep-ph].
- [39] S. Bailey, T. Cridge, L. A. Harland-Lang, A. D. Martin, and R. S. Thorne, *Eur. Phys. J. C* **81**, 341 (2021), arXiv:2012.04684 [hep-ph].
- [40] M. Butenschoen and B. A. Kniehl, *Phys. Rev. D* **84**, 051501 (2011), arXiv:1105.0820 [hep-ph].
- [41] K.-T. Chao, Y.-Q. Ma, H.-S. Shao, K. Wang, and Y.-J. Zhang, *Phys. Rev. Lett.* **108**, 242004 (2012), arXiv:1201.2675 [hep-ph].
- [42] B. Gong, L.-P. Wan, J.-X. Wang, and H.-F. Zhang, *Phys. Rev. Lett.* **110**, 042002 (2013), arXiv:1205.6682 [hep-ph].

- [43] R. Sharma and I. Vitev, *Phys. Rev. C* **87**, 044905 (2013), [arXiv:1203.0329 \[hep-ph\]](#).
- [44] N. Brambilla, H. S. Chung, A. Vairo, and X.-P. Wang, *Phys. Rev. D* **105**, L111503 (2022), [arXiv:2203.07778 \[hep-ph\]](#).

SUPPLEMENTAL MATERIAL

As the supplemental material of the paper, we provide all the technical details below.

I. EVALUATION OF SOFT GLUON RADIATIONS

In this section, we provide detailed derivations of the soft gluon radiation contributions obtained by integrating the relevant rapidity phase space. This requires discussing four functions of the kind presented in Eq. (3): $S_g(p_2, k_j)$, $S_g(p_2, k_\psi)$, $S_g(k_j, k_\psi)$, and $S_g(k_\psi, k_\psi)$.

Integral of $S_g(p_2, k_j)$. We start with the first one on the list, which is the only one contributing to the CS channel. Although its integral was relevant, and therefore computed, in other works [21, 22, 25–28], for completeness we report the calculation in the following. To better analyze the physical content of this derivation, we can divide $S_g(p_2, k_2)$ into three contributions as follows

$$\begin{aligned} S_g(p_2, k_j) &= \frac{2(p_2 \cdot k_j)}{(p_2 \cdot k_g)(k_j \cdot k_g)} \\ &= \frac{2}{|\vec{k}_{g\perp}|^2} \frac{e^{\Delta y_g}}{\cosh(\Delta y_g) - \cos(\Delta\phi_g)} \\ &\approx \frac{2}{|\vec{k}_{g\perp}|^2} \left(1 + \frac{\sinh(\Delta y_g)}{\cosh(\Delta y_g) - \cos(\phi)} \right. \\ &\quad \left. + \frac{\cos(\phi)}{\cosh(\Delta y_g) - \cos(\phi)} \right), \end{aligned} \quad (15)$$

where we have defined $\Delta y_g = y_g - y_j$, namely the difference between the emitted soft gluon and jet rapidities. The first term in the bracket of Eq. (15) leads to the double-logarithm. The second one, being an odd function of Δy_g , receives contributions only from the boundaries of the integration region, which causes the presence of the additional logarithmic term, $\ln(\hat{t}/\hat{u})$, in Eq. (4). The last term in Eq. (15) contains the jet contribution to azimuthal angular asymmetries.

In particular, this distribution is described by the function

$$\begin{aligned} I_j(R, \phi) &= \int d\Delta y_g \frac{\cos(\phi)}{\cosh(\Delta y_g) - \cos(\phi)} \\ &\quad - \frac{|\vec{k}_{g\perp}|^2}{2} \int d\Delta y_g S_g(p_2, k_j) \Theta(\Delta_{k_g k_j} < R^2) \\ &= \int d\Delta y_g \frac{\cos(\phi)}{\cosh(\Delta y_g) - \cos(\phi)} \Theta(\Delta_{k_j k_g} > R^2) \\ &\quad - 2\sqrt{R^2 + \phi^2}, \end{aligned} \quad (16)$$

where $\Theta(\Delta_{k_j k_g} \lesseqgtr R^2)$ implies that the integration is restricted inside ($<$) or outside ($>$) the rapidity region occupied by the jet cone with size R , namely

$$|\Delta y_g| > \sqrt{R^2 + \phi^2}. \quad (17)$$

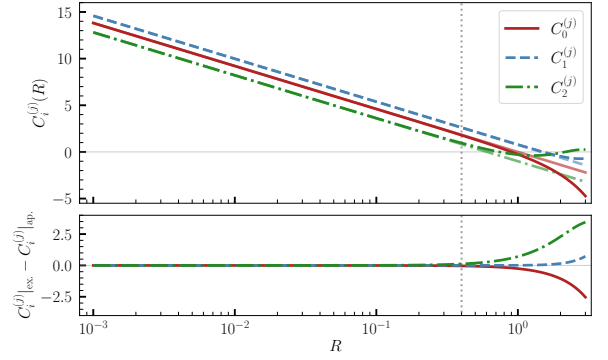


FIG. 4. Dependence of the first coefficients of Eq. (5) with respect to R . In the upper panel we show both the exact result obtained from a numerical computation (full color) and the approximated one given in Eq. (18) (softer color). In the lower panel, we present the difference between the two. The vertical dotted line corresponds to $R = 0.4$, beyond which the approximation fails.

For a general R , the Fourier expansion of $I_j(R, \phi)$ (Eq. (5)) is manageable only via computational methods. However, the analytical evaluation of this expansion within the small- R limit is possible. Hence we find

$$\begin{aligned} I_j(R, \phi) &= \ln \frac{1}{R^2} + 2 \cos(\phi) \left(\ln \frac{1}{R^2} + 2 \ln(4) - 2 \right) \\ &\quad + 2 \cos(2\phi) \left(\ln \frac{1}{R^2} - 1 \right) + \dots, \end{aligned} \quad (18)$$

from which it is evident that there is a non-negligible $\cos(\phi)$ azimuthal angular dependence in $I_j(R, \phi)$.

In Fig. 4, we show how the first three coefficients of the Fourier expansion behave with respect to R . From this figure, we conclude that the approximation used in Eq. (18) is reasonably adequate for $R < 0.4$.

Integral of $S_g(p_2, k_\psi)$. Similarly to $S_g(p_2, k_j)$, we divide $S_g(p_2, k_\psi)$ in the following three terms

$$\begin{aligned} S_g(p_2, k_\psi) &= \frac{2(p_2 \cdot k_\psi)}{(p_2 \cdot k_g)(k_\psi \cdot k_g)} \\ &= \frac{2}{|\vec{k}_{g\perp}|^2} \frac{e^{\Delta y_{g\psi}}}{\sqrt{1 + m_{\psi\perp}^2} \cosh(\Delta y_{g\psi}) - \cos(\Delta\phi_{g\psi})} \\ &\approx \frac{2}{|\vec{k}_{g\perp}|^2} \left(1 + \frac{\sqrt{1 + m_{\psi\perp}^2} \sinh(\Delta y_{g\psi})}{\sqrt{1 + m_{\psi\perp}^2} \cosh(\Delta y_{g\psi}) + \cos(\phi)} \right. \\ &\quad \left. - \frac{\cos(\phi)}{\sqrt{1 + m_{\psi\perp}^2} \cosh(\Delta y_{g\psi}) + \cos(\phi)} \right), \end{aligned} \quad (19)$$

where we have defined $\Delta y_{g\psi} = y_g - y_\psi$, namely the difference between the emitted soft gluon and J/ψ rapidities, and $\Delta\phi_{g\psi} = \phi_g - \phi_\psi = \phi_g$ in a frame where $\phi_\psi = 0$. As for Eq. (15), the first term in the bracket of Eq. (19) leads to the double-logarithm while the second one receives

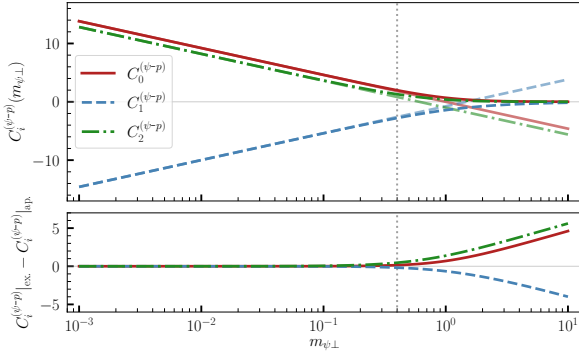


FIG. 5. Dependence of the first coefficients of Eq. (22) with respect to $m_{\psi\perp}$. Vertical dotted line corresponds to $m_{\psi\perp} = 0.4$. Panels follow the same logic as Fig. 4.

contributions only from the boundaries of the integration region, providing the logarithms: $\ln \frac{\hat{u}}{\hat{t}} + \ln \frac{1-M_\psi^2/\hat{u}}{1-M_\psi^2/\hat{t}}$. These, once combined with the other analogous logarithms arising from $S_g(p_2, k_j)$, cause the presence of the second term in Eq. (7). The last term in Eq. (19) contains part of the J/ψ contribution to azimuthal angular asymmetries.

We identify this angular distribution as

$$I_{\psi-p}(m_{\psi\perp}, \phi) = \int d\Delta y_{g\psi} \left[-\frac{\cos(\phi)}{\sqrt{1+m_{\psi\perp}^2} \cosh(\Delta y_{g\psi}) + \cos(\phi)} \right] \quad (20)$$

Note that the presence of the mass in the denominator

acts as a regulator, and therefore $I_{\psi-p}$ is continuous for all values of ϕ . Moreover, when evaluated within the jet rapidity region, Eq. (19) leads to

$$I_{\psi-p}^{\text{jet}}(R, m_{\psi\perp}, \Delta y, \phi) = \frac{|\vec{k}_{g\perp}|^2}{2} \int d\Delta y_g S_g(p_2, k_\psi) \Theta(\Delta_{k_g k_j} < R^2), \quad (21)$$

which not only depends on both parameters R and $m_{\psi\perp}$, but on the rapidity difference $\Delta y = y_\psi - y_j$ too. The distribution in Eq. (20) can be expanded according to Eq. (8), which leads to

$$I_{\psi-p}(m_{\psi\perp}, \phi) = C_0^{(\psi-p)}(m_{\psi\perp}) + 2 \sum_{n=1}^{\infty} C_n^{(\psi-p)}(m_{\psi\perp}) \cos(n\phi). \quad (22)$$

These coefficients can be analytically evaluated only in the small- $m_{\psi\perp}$ limit, for which

$$I_{\psi-p}(m_{\psi\perp}, \phi) = \ln \frac{1}{m_{\psi\perp}^2} - 2 \cos(\phi) \left(\ln \frac{1}{m_{\psi\perp}^2} + 2 \ln(4) - 2 \right) + 2 \cos(2\phi) \left(\ln \frac{1}{m_{\psi\perp}^2} - 1 \right) + \dots \quad (23)$$

Fig. 5 shows the dependence of the first three coefficients with respect to $m_{\psi\perp}$, together with the reliability of the approximation introduced in Eq. (23).

Integral of $S_g(k_j, k_\psi)$. Compared to the previous functions, deriving the azimuthal distribution arising from $S_g(k_j, k_\psi)$ requires some extra care. Firstly, we recast the function as follows

$$S_g(k_j, k_\psi) = \frac{2(k_j \cdot k_\psi)}{(k_j \cdot k_g)(k_\psi \cdot k_g)} \approx \frac{2}{|\vec{k}_{g\perp}|^2} \frac{\sqrt{1+m_{\psi\perp}^2} \cosh(\Delta y) + 1}{\left[\cosh(\Delta y_g) - \cos(\phi) \right] \left[\sqrt{1+m_{\psi\perp}^2} \cosh(\Delta y_{g\psi}) + \cos(\phi) \right]} = \frac{2}{|\vec{k}_{g\perp}|^2} \left(\frac{\cos(\phi)}{\cosh(\Delta y_g) - \cos(\phi)} - \frac{\cos(\phi)}{\sqrt{1+m_{\psi\perp}^2} \cosh(\Delta y_{g\psi}) + \cos(\phi)} + \widehat{S}_g(k_j, k_\psi) \right), \quad (24)$$

where we remark that $\Delta y = y_\psi - y_j$, $\Delta y_g = y_g - y_j$ and $\Delta y_{g\psi} = y_j - y_\psi$, with y_j , y_ψ and y_g being respectively the jet, J/ψ and emitted soft gluon rapidities. The first two terms in the last line of Eq. (24) coincide with the last

terms of Eqs. (15) and (19), respectively, and thus remove the double counting in the azimuthal dependences. The last term, which is explicitly given by

$$\widehat{S}_g(k_j, k_\psi) = \frac{1 + \sqrt{1 + m_{\psi\perp}^2} \cosh(\Delta y)}{\cosh(\Delta y_g) + \sqrt{1 + m_{\psi\perp}^2} \cosh(\Delta y_{g\psi})} \left(\frac{1}{\cosh(\Delta y_g) - \cos(\phi)} + \frac{1}{\sqrt{1 + m_{\psi\perp}^2} \cosh(\Delta y_{g\psi}) + \cos(\phi)} \right) - \frac{\left(\cosh(\Delta y_g) + \sqrt{1 + m_{\psi\perp}^2} \cosh(\Delta y_{g\psi}) \right) \cos(\phi)}{\cosh(\Delta y_g) + \sqrt{1 + m_{\psi\perp}^2} \cosh(\Delta y_{g\psi})} \left(\frac{1}{\cosh(\Delta y_g) - \cos(\phi)} - \frac{1}{\sqrt{1 + m_{\psi\perp}^2} \cosh(\Delta y_{g\psi}) + \cos(\phi)} \right), \quad (25)$$

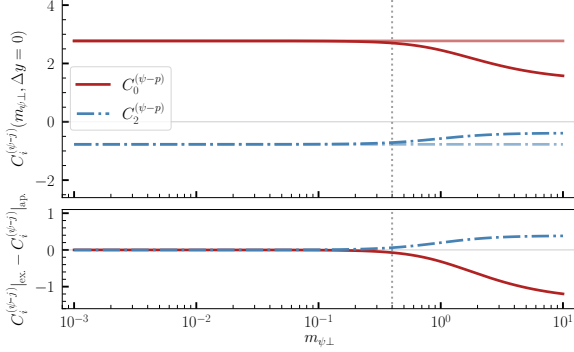


FIG. 6. Dependence of the first coefficients of Eq. (29) with respect to $m_{\psi\perp}$ and for $\Delta y = 0$. The coefficient C_1 , being zero, is not shown here. Vertical dotted line corresponds to $m_{\psi\perp} = 0.4$. Panels follow the same logic as Fig. 4.

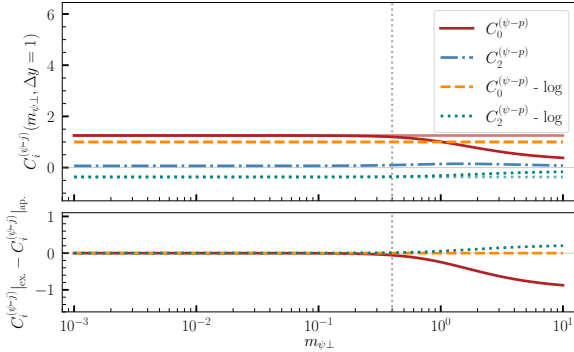


FIG. 7. Same as Fig. 6 but for $\Delta y = 1$. At variance with the previous figure, we have that the coefficients include extra logarithms (see Eq. (30)), which are shown separately.

produces the unique azimuthal distribution of $S_g(k_j, k_\psi)$.

Therefore, we identify the azimuthal distribution driven by the first two terms as

$$I_{\psi-j}(R, m_{\psi\perp}, \phi) = \int dy_g \left(\frac{\cos(\phi)}{\cosh(\Delta y_g) - \cos(\phi)} - \frac{\cos(\phi)}{\sqrt{1 + m_{\psi\perp}^2} \cosh(\Delta y_{g\psi}) + \cos(\phi)} \right), \quad (26)$$

which is independent of Δy and part of I_ψ in Eq. (7) (see also the end of this section), while the last term gives

$$I_{\psi-j}(m_{\psi\perp}, \Delta y, 2\phi) = \int dy_g \widehat{S}_g(k_j, k_\psi), \quad (27)$$

which is exactly the same of Eq. (7). Moreover, $S_g(k_j, k_\psi)$ provides another azimuthal distribution when evaluated within the jet region

$$I_{\psi-j}^{\text{jet}}(R, m_{\psi\perp}, \Delta y, \phi) = \frac{|\vec{k}_{g\perp}|^2}{2} \int d\Delta y_g S_g(k_j, k_\psi) \Theta(\Delta_{k_j k_\psi} < R^2). \quad (28)$$

Among these three distribution, Eq. (27) is the most interesting. Note that this distribution only contributes to the even modes of the Fourier expansion and does not depend on the jet variable R , since the integration of $\widehat{S}_g(k_j, k_\psi)$ is continuous at $\phi = 0$. However, it presents an additional dependence on the rapidity difference Δy , which affects its harmonic expansion, given by

$$I_{\psi-j}(m_{\psi\perp}, \Delta y, 2\phi) = C_0^{(\psi-j)}(m_{\psi\perp}, \Delta y) + 2 \sum_{n=1}^{\infty} C_{2n}^{(\psi-p)}(m_{\psi\perp}, \Delta y) \cos(2n\phi). \quad (29)$$

In particular, depending on the value of Δy we can have additional logarithms of \hat{u}/\hat{t} within the coefficients. Moreover, the closer the two outgoing particles are to the production axis (namely $|\Delta y| \rightarrow \infty$), the less relevant the angular distribution in $I_{\psi-j}(m_{\psi\perp}, \Delta y, 2\phi)$ becomes, with its sole contribution being restricted to the logarithm of \hat{u}/\hat{t} in the constant term. To see this effect, we consider the analytical expansion in the small- $m_{\psi\perp}$ limit for two values of Δy , namely $\Delta y = 0$ and $\Delta y = 1$:

$$\begin{aligned}
I_{\psi-j}(m_{\psi\perp}, \Delta y = 0, 2\phi) &= 2 \ln(4) - 4 \cos(2\phi) (\ln(4) - 1) + \dots, \\
I_{\psi-j}(m_{\psi\perp}, \Delta y = 1, 2\phi) &= 2 \left[2 \left(\ln(1+e) - 1 \right) - \ln \frac{\hat{u}}{\hat{t}} - \frac{1}{2} \ln \frac{1 - M_\psi^2/\hat{u}}{1 - M_\psi^2/\hat{t}} \right] \\
&\quad - \frac{4}{e} \cos(2\phi) \left[(1+e^2) \left(\ln(1+e) - 1 \right) + e - \ln \frac{\hat{u}}{\hat{t}} - \frac{1}{2} \ln \frac{1 - M_\psi^2/\hat{u}}{1 - M_\psi^2/\hat{t}} \right] + \dots
\end{aligned} \tag{30}$$

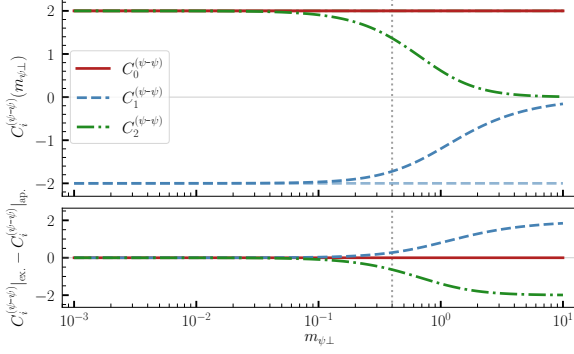


FIG. 8. Dependence of the first coefficients of Eq. (34) with respect to $m_{\psi\perp}$. Note that the coefficient C_0 does not vary with $m_{\psi\perp}$. Vertical dotted line corresponds to $m_{\psi\perp} = 0.4$. Panels follow the same logic as Fig. 4.

The complete dependence of the first coefficients of Eq. (29) for the same values of Δy is shown in Figs. 6 and 7.

Integral of $S_g(k_\psi, k_\psi)$. The function $S_g(k_\psi, k_\psi)$, non-zero only for massive particles, is given by

$$\begin{aligned}
S_g(k_\psi, k_\psi) &\approx \frac{2}{|\vec{k}_{g\perp}|^2 \left(\sqrt{1 + m_{\psi\perp}^2} \cosh(\Delta y_{g\psi}) + \cos(\phi) \right)^2}, \tag{31}
\end{aligned}$$

where we recall that $m_{\psi\perp} = M_\psi/|\vec{P}_\perp|$ with M_ψ being the J/ψ mass, and $\Delta y_{g\psi}$ is the rapidity difference between the soft gluon and the quarkonium.

The azimuthal distribution arising from $S_g(k_\psi, k_\psi)$ is identify by

$$\begin{aligned}
I_{\psi-\psi}(m_{\psi\perp}, \phi) &= \int d\Delta y_{g\psi} \frac{m_{\psi\perp}^2}{\left(\sqrt{1 + m_{\psi\perp}^2} \cosh(\Delta y_{g\psi}) + \cos(\phi) \right)^2}, \tag{32}
\end{aligned}$$

Moreover, when evaluated within the jet region, $S_g(k_\psi, k_\psi)$ generates

$$\begin{aligned}
I_{\psi-\psi}^{\text{jet}}(R, m_{\psi\perp}, \Delta y, \phi) &= \frac{|\vec{k}_{g\perp}|^2}{2} \int d\Delta y_g S_g(k_\psi, k_\psi) \Theta(\Delta_{k_g k_j} < R^2). \tag{33}
\end{aligned}$$

The harmonic expansion of Eq. (32), following that of Eq. (8), is given by

$$\begin{aligned}
I_{\psi-\psi}(m_{\psi\perp}, \phi) &= C_0^{(\psi-\psi)}(m_{\psi\perp}) + 2 \sum_{n=1}^{\infty} C_n^{(\psi-\psi)}(m_{\psi\perp}) \cos(n\phi). \tag{34}
\end{aligned}$$

It is interesting to notice that these coefficients are non-zero for all $m_{\psi\perp}$. In particular, we have residual contributions in the small- $m_{\psi\perp}$ limit, with $C_0^{(\psi-\psi)}, C_2^{(\psi-\psi)} \rightarrow 2$ and $C_1^{(\psi-\psi)} \rightarrow -2$, which is expected due to the singular behaviour of $I_{\psi-\psi}$ at $\phi = \pi$.

For completeness, Fig. 8 shows the exact dependence of the coefficients on $m_{\psi\perp}$. From this figure we understand that $C_0^{(\psi-\psi)}$ is independent of $m_{\psi\perp}$, whereas $C_1^{(\psi-\psi)}$ and $C_2^{(\psi-\psi)}$ are negligible when $m_{\psi\perp} \approx 1$.

Overall azimuthal distribution. By combining all the soft gluon emission evaluated above, one gets the differential cross section as a function of q_\perp given in Eq. (9), where the expansion in terms of $\cos(n\phi)$ harmonics has already being performed. The coefficients of this expansion depend on the production mechanism considered. For the CS channel, we have that $C_n^{(1)}$ are directly related to the Fourier expansion of I_j in Eq. (5). On the other hand, in the CO channel the coefficients $C_n^{(8)}$ are driven by all distributions in Eq. (7). More specifically, we have:

- $I_\psi(m_{\psi\perp}, \phi) = I_{\psi-p}(m_{\psi\perp}, \phi) - \frac{1}{2} I_{\psi-\psi}(m_{\psi\perp}, \phi)$;
- $I_{\psi-j}(R, m_{\psi\perp}, \Delta y, 2\phi)$ is given in Eq. (27);
- $I_\psi^{\text{jet}} = I_{\psi-p}^{\text{jet}} + I_{\psi-j}^{\text{jet}} - I_{\psi-\psi}^{\text{jet}} - I_j^{\text{jet}}(R, \phi)$, where I_j^{jet} is the contribution of I_j inside the jet region (namely the term in the second line of Eq. (16)).

In Fig. 9 we present the dependence of the coefficients with respect to R and $m_{\psi\perp}$ for $\Delta y = 0$. From a direct comparison between the CS and CO channels, it is evident that predictions that include the CO mechanism are significantly different from those exclusively driven by the CS one.

II. AZIMUTHAL ASYMMETRIES IN THE CS AND CO CHANNELS SEPARATELY

In this section we present direct comparisons between the CS and CO mechanisms, providing more insights on

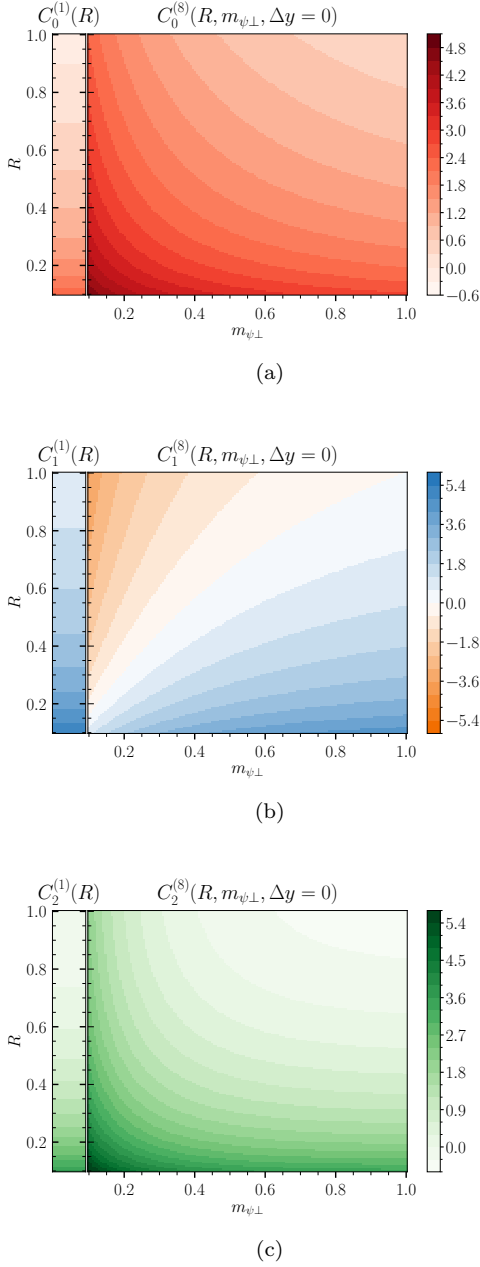


FIG. 9. Dependence of the first coefficients on the jet size R and the variable $m_{\psi\perp}$ in the CO channel for transverse production ($\Delta y = 0$). A comparison with the CS channel, for which coefficients solely depend on R , is given by the column on the left.

the results shown in Fig. 3.

In Fig. 10 we present the normalized differential cross section within both the CS and CO channels and for the same kinematics considered for Fig. 3. The CO channel has a much wider distribution as compared to the CS one as a result of the final state gluon radiation associated with the heavy quark pair, which leads to a significant difference in the associated $C_0^{(c)}$ coefficients (see Table I). Note that, although the normalized distribu-

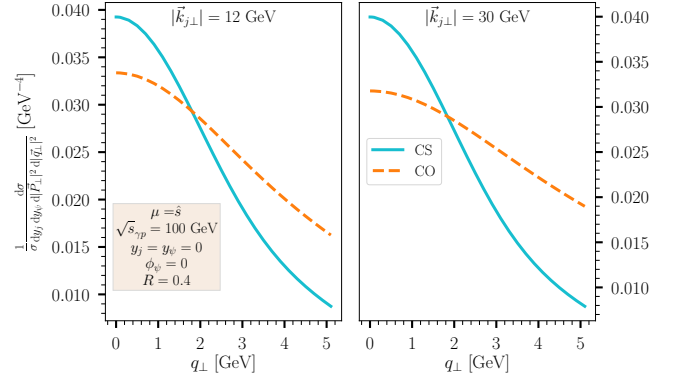


FIG. 10. Normalized differential cross section of isotropic J/ψ plus jet photoproduction at $\sqrt{s}_{\gamma p} = 100 \text{ GeV}$ in a frame where the azimuthal angle of \vec{P}_\perp is zero and $y_j = y_\psi = 0$. We considered two values of $|\vec{k}_{j\perp}|$, while $R = 0.4$. Solid cyan lines are obtained employing the CS channel, whereas the dashed orange lines the CO one.

tions are similar for the two values of $|\vec{k}_{j\perp}|$ taken, the differential cross sections decrease significantly (approximately by an order of magnitude). It is worth mentioning that Fig. 10 is obtained for $y_j = y_\psi = 0$ and different rapidities values can slightly modify the picture, e.g. less broadened distributions for $y_j = 1$. Nonetheless, other choices of y_j and y_ψ do not spoil the main conclusion of Fig. 10, namely that we identify different shapes of the normalized differential cross sections within the CS and CO mechanisms.

Moving to the asymmetries, in Fig. 11 we present, as functions of q_{\perp} and for the same kinematic choices of Fig. 3, $\langle \cos(\phi) \rangle$ and $\langle \cos(2\phi) \rangle$ predictions in the CS and CO channels. For comparison, we also show the fixed-order results. In this figure, the behaviors of the resummed asymmetries within the CS and CO mechanisms are analogous to those of the CSM and NRQCD in Fig. 3. Thus, we may conclude that the NRQCD outcomes are mostly driven by the CO channel, at least for the kinematics considered.

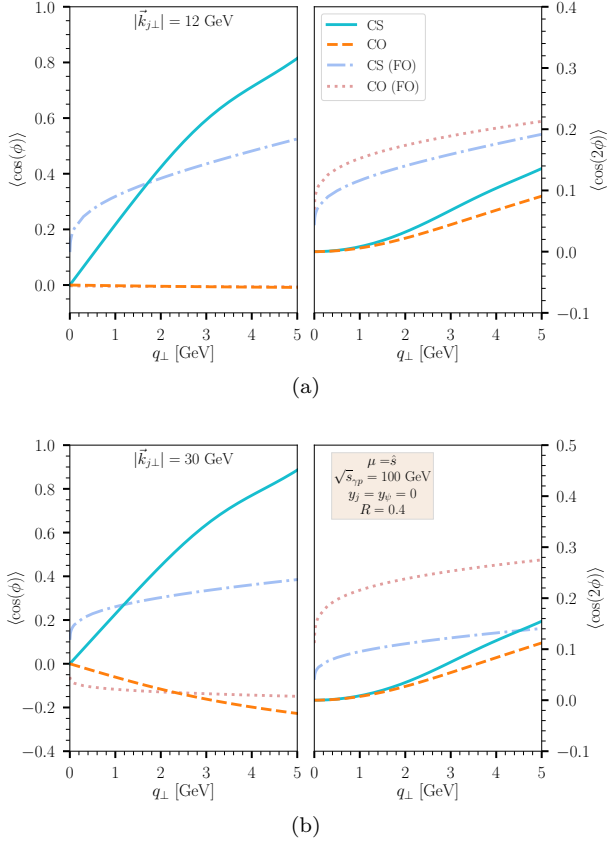


FIG. 11. Averaged azimuthal asymmetries for J/ψ plus jet photoproduction at $\sqrt{s_{\gamma p}} = 100$ GeV obtained within the CS (solid cyan line) and CO (dashed orange line) mechanisms. The dash-dotted blue and dotted red lines are the fixed-order results for the CS and CO channels, respectively. The curves in the top panel (11a) are evaluated at $|\vec{k}_{j\perp}| = 12$ GeV, whereas those in the bottom panel (11b) at $|\vec{k}_{j\perp}| = 30$ GeV. Jet size is $R = 0.4$ in both panels.